ARTICLE

Real-time TEM observations of ice formation in graphene liquid cell

Abhijit H. Phakatkar,*[a] Constantine M. Megaridis,*[b] Tolou Shokuhfar,*[a] Reza Shahbazian-Yassar*[b]

The study of ice nucleation and growth at the nanoscale is of utmost importance in geological and atmospheric sciences. However, existing transmission electron microscopy (TEM) approaches have been unsuccessful in imaging ice formation directly. Herein, we demonstrate how radical scavengers -such as TiO_2- encased with water in graphene liquid cells (GLCs) facilitate the observation of ice nucleation phenomena at low temperatures. Atomic resolution imaging reveals the nucleation and growth of cubic ice phase crystals at close proximity to TiO_2-water nanointerfaces at low temperatures. Interestingly, both heterogeneously and homogeneously nucleated ice crystals exhibited this cubic phase. Ice crystal nuclei were observed to be more stable at the TiO_2-water nanointerface, as compared with crystals in the bulk liquid (homogeneous nucleation), suggesting the radical scavenging efficacy of TiO_2 nanoparticles mitigating the electron beam by-products. The present work demonstrates that the use of radical scavengers in GLC TEM has great promise in unveiling the nanoscale pathways for ice nucleation and growth dynamic events.

Introduction

Ice nucleation and growth are subjects of considerable interest owing to their extreme importance in geological, biological, and atmospheric sciences.[1-4] Ice nucleation can follow two pathways, namely homogeneous and heterogeneous nucleation. Mineral dust aerosols are among the most prevalent sources of heterogeneous ice nucleation in clouds.[5] Aluminum oxide (Al_2O_3), titanium dioxide (TiO_2), magnesium oxide (MgO), iron oxides (Fe_3O_4, Fe_2O_3), and silicon dioxide (SiO_2) are well-known metal oxide atmospheric constituents of mineral dust, which are responsible for heterogeneous ice nucleation.[6-8] At the metal oxide-water interface, primarily adsorbed water with successive dissociation is considered to be a crucial step for heterogeneous ice nucleation.[9] The strong interaction among hydrogen bonds of the water molecule and metal-oxide surface oxygen results in extraction of hydrogen molecules and hence, adsorption of water-molecule oxygen on metal cations.[10] With the defect sites increasing the density of adsorbed water molecules, surface hydroxyl groups are responsible for enhanced chemical affinity for ice and specific crystal lattice plane directions, which serve as active sites on metal oxide surfaces for ice nucleation.[11]

The ice-forming activity of metal oxides has been evaluated using different experimental bulk characterization techniques. Souda *et al.*[8] used a reflection high-energy electron diffraction (RHEED) technique to evaluate the epitaxial growth of cubic ice crystal phase at a TiO_2 nanointerface. Kiselev *et al*.[11] utilized environmental scanning electron microscopy (ESEM) to investigate the ice forming activity of feldspar (rock-forming mineral) confirming defects acting as heterogeneous ice nucleation sites. Jia *et al*.[12] investigated ultrasound-controlled heterogeneous ice nucleation on TiO_2 nanoparticles. Even though efforts are ongoing to study ice nucleation on metal oxides, existing experimental studies are limited to the micron scale. At present, sub-micron level ice nucleation pathways and associated crystal orientation events at complex interfaces are predominantly studied

using molecular simulation theoretical models.[13-15] There exists a knowledge gap with currently available experimental approaches to comprehend ice nucleation events at nanointerfaces.

Transmission electron microscopy (TEM) and associated selected area electron diffraction (SAED) have shown potential to study ice crystal phases. Hexagonal and cubic ice crystal phases at distinct cryogenic temperatures were evaluated using low-magnification TEM and SAED techniques.[16, 17] Kouchi *et al.*[18] used TEM to demonstrate substrate-dependent ice nucleation and crystallization from water vapor deposition at 130 K. Recently, Kato *et al.*[19] reported a strategy to maintain ultrathin ice between bilayer graphene using a cryo-TEM approach.

In addition to conventional TEM techniques, *in-situ* liquid TEM is an emerging approach that has gained traction in the scientific community to study the ice crystallization process. For real-time high-resolution TEM studies, *in-situ* graphene liquid cell (GLC) TEM has exhibited tremendous potential. It is possible to acquire atomic resolution imaging with higher signal-to-noise ratio in GLC, while mitigating the electron-beam-induced charging effects.[20] The properties of graphene attributing to electrical conductivity, high yield strength, electron transparency, flexibility, and impermeability gives it unique advantages for TEM studies.[21] Graphene monolayers in *in-situ* GLC-TEM can maintain the aqueous environment for dynamic event observations at the nanoscale. [22, 23] Algara-Siller *et al*.[24] evaluated the square ice crystal phase formed under pressure in graphene nanocapillaries via in-situ liquid TEM, although some doubts were casted on the results.[25, 26] Despite the recent advances in *in-situ* TEM, studying ice nucleation and growth remains a grand challenge due to intense radiolysis associated with the interaction between the electron beam and water molecules.[23, 27] In our earlier work[28], using electron energy loss spectroscopy (EELS) and GLC-TEM, we demonstrated the change in hydrogen bonding distances in water molecules (resembling ice-like organization of water molecules) confined in graphene nanocapillaries at cryogenic temperatures.

In the present study, we report that radical scavengers -such as titanium dioxide (TiO_2)- can be effective in mitigating radiolysis, while enabling studies of ice crystal nucleation at the nanointerface of water and metal nanoparticles in a cold-stage TEM holder maintained at cryogenic temperatures. Atomic resolution imaging reveals nucleation and growth of cubic-phase ice crystals at the surface of anatase TiO_2 nanoparticles. Fast Fourier Transform (FFT) analysis confirms the predominance of characteristic (220) lattice planes of cubic phase ice crystals affiliated with 2.2 Å d-spacings. The atomic resolution *in-situ* liquid TEM results also provide insights on electron beam-induced dissolution of ice crystals. The key dynamic events of cubic-phase single ice crystal nucleation and growth and ice-crystal growth via oriented attachment of multiple crystallites along $(2\bar{2}0)$ active facets are evaluated in detail. The present work demonstrates that the use of radical scavengers can be effective for *in-situ* TEM studies of ice nucleation and growth dynamics that are important for climate change, agriculture and microbial ecology, as well as industrial cooling technologies.

Results and discussion

Figure 1 presents the overall approach of the present study which focuses on ice crystal growth in GLC-TEM. **Figure 1a** is a schematic representation

of ice crystal nucleation and growth events in the presence of TiO_2 nanoparticles encapsulated in GLC nano-vessels at cryogenic temperatures. To study the ice nucleation with TEM resolution, a cold-stage TEM holder was utilized to achieve low temperatures.

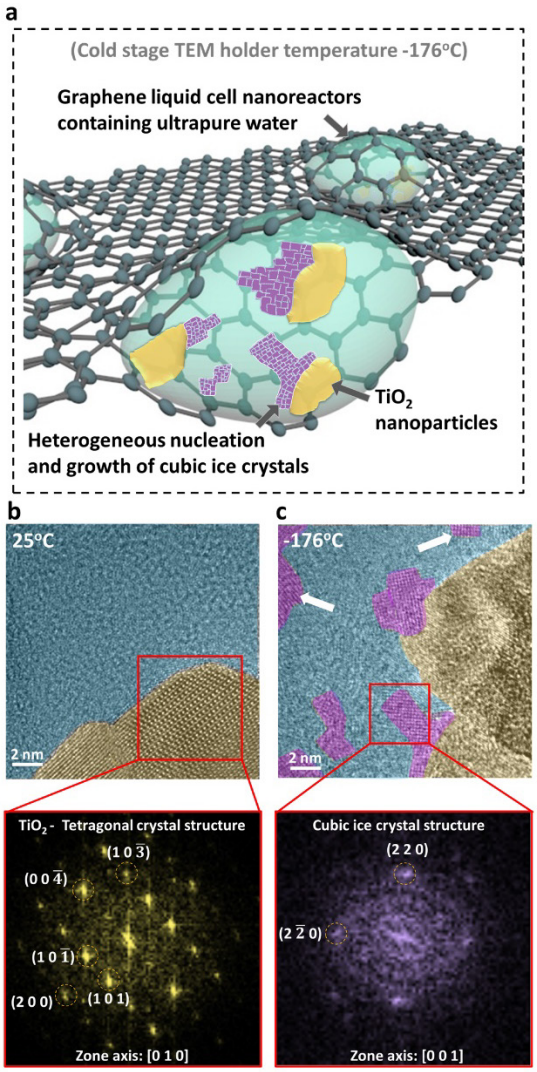

Figure 1. Ice crystal growth in GLC at cryogenic temperatures. (a) Schematic representation of ice crystal (in purple) nucleation and growth events in the presence of TiO_2 nanoparticles (in yellow). (b) TiO_2 nanoparticles in GLC aqueous environment at room temperature, along with FFT analysis confirming the tetragonal crystal structure of anatase TiO_2 along the [010] zone axis. (c) Ice crystal growth at the TiO_2-water nanointerface along with FFT pattern confirming the cubic phase of ice crystals along the [001] zone axis. The TiO_2 nanoparticles, ice, and water have been false-colored in gold, purple, and cyan, respectively, for better visualization.

TiO_2 was selected as a strong radical scavenger additive and its usefulness in the study of heterogeneous ice nucleation on metal oxide interfaces. In other recent work, radical scavenging of Ta-TiO_x nanoparticles was demonstrated.[29] Carey *et al*.[30] reported that anatase TiO_2 can trap electrons at low coordinated surface Ti cation sites at the bottom of their conduction band. Additionally, active sites on a Ti surface can adsorb and neutralize reaction of radicals.[31] Additionally, graphene possesses inherent radical scavenging capability, where sp^2 carbon sites play a crucial role.[32, 33] Radical species form adducts with sp^2 carbon sites of graphene by delocalizing electron spin via electron transfer, which further neutralizes radical species.[33, 34] Results indicate that TiO_2 nanoparticles encapsulated in GLC-contained aqueous media may play a major role in reducing electron-beam-induced damage.

Figure 1b shows a TEM micrograph of TiO_2-water interface in the GLC when the TEM holder was at room temperature (25°C) prior to cooling. The corresponding Fast Fourier Transform (FFT) analysis confirms the tetragonal crystal structure of the anatase TiO_2 nanoparticles. At 25°C, ice crystals were not present at the TiO_2-water interface in the GLC. The TiO_2 nanoparticle/water interface at 25°C can be observed in **Video S1**. **Figure 1c** presents a TEM micrograph of ice crystals nucleated at the TiO_2-water interface and at nearby locations in the water bulk. The corresponding FFT pattern in Fig. 1c confirms the cubic phase of heterogeneously grown ice crystals with prominent {220} family of lattice planes having 2.2 Å d-spacing. The homogeneously grown ice crystals are marked with the white arrows. **Video S2** shows multiple homogeneously grown ice crystals observed in the vicinity of TiO_2 nanoparticles. Interestingly, both the heterogeneously and homogeneously grown ice crystals were consistent with the cubic phase. The local cryogenic temperature conditions and the pressure inside the GLC are possibly the driving factors for maintaining the cubic phase of ice

crystals.[17] The detailed ice nucleation dynamic events are discussed further in the following sections.

In the environment, ice nucleation is predominantly occurring by heterogeneous pathways, where active sites on ice nucleating particles play a crucial role in ice nucleation.[11] Kislev *et al.*[11] showed that high free surface energy is an additional factor in promoting heterogeneous ice nucleation. Moreover, intrinsic factors, such as surface morphological irregularities, surface defects increasing localized density of adsorbed water molecules, surface hydroxyl groups improving the binding affinity of water molecules, and crystal lattice match promoting epitaxial growth of ice nuclei, drive heterogeneous ice nucleation.[35-39]

Figure 2 shows time-sequenced TEM micrographs of real-time heterogeneous nucleation and ice crystal growth at a TiO_2-water nanointerface when the GLC was at cryogenic temperature. These TEM micrographs were acquired from **Video S3**. In **Figure 2a**, the progression of nucleation and growth of a single ice crystal at the TiO_2-water interface can be observed. The corresponding FFT analyses from the highlighted regions are presented in **Figure 2b**. At 0.25 s, there are no ice nuclei present. The corresponding amorphous central region can be observed in the FFT pattern, where bright spots representing crystal lattice planes are absent. From 1s to 23 s, nucleation and stable growth of an ice crystal can be observed. The corresponding FFT pattern confirmed that the cubic ice phase was maintained throughout the progression. Ice crystal growth was observed along the $[2\bar{2}0]$ direction with the [001] zone axis. The {220} family of planes corresponding to 2.2 Å d-spacing was consistently present. Additionally, to confirm the absence of a contaminant, *in-situ* GLC STEM-EELS was utilized to probe the energy range from 140 eV to 730 eV. The STEM-EELS high-energy loss spectrum (**Figure S1**) confirmed the presence of oxygen (associated with water) and carbon K-edges (associated with graphene) at 532 eV and 284 eV, respectively. The absence of a chlorine L-edge at 200 eV suggests the lack of chloride salts in water. The corresponding STEM-EELS elemental mapping confirmed the presence of water in the graphene nanocapillaries.

FFT analysis of the growing ice crystal at atomic resolution confirmed the predominantly cubic phase of ice. There exists a possibility of a stacking disorder in cubic ice crystals. Lupi *et al*.[40] demonstrated the seamless stacking of cubic and hexagonal crystal phases using molecular dynamics simulations. Cubic ice crystal phases are likely to undergo stacking disorder with hexagonal ice layers, resulting in the growth of ice nuclei by stacking simultaneously in multiple directions.[14, 40] In the present study, due to the experimentation limitations, only the bright spots associated with the cubic phase of ice in the FFT patterns were resolved. As revealed by FFT pattern analysis, no prominent sub-nanometer scale hexagonal stacking disorder was observed in this sample.

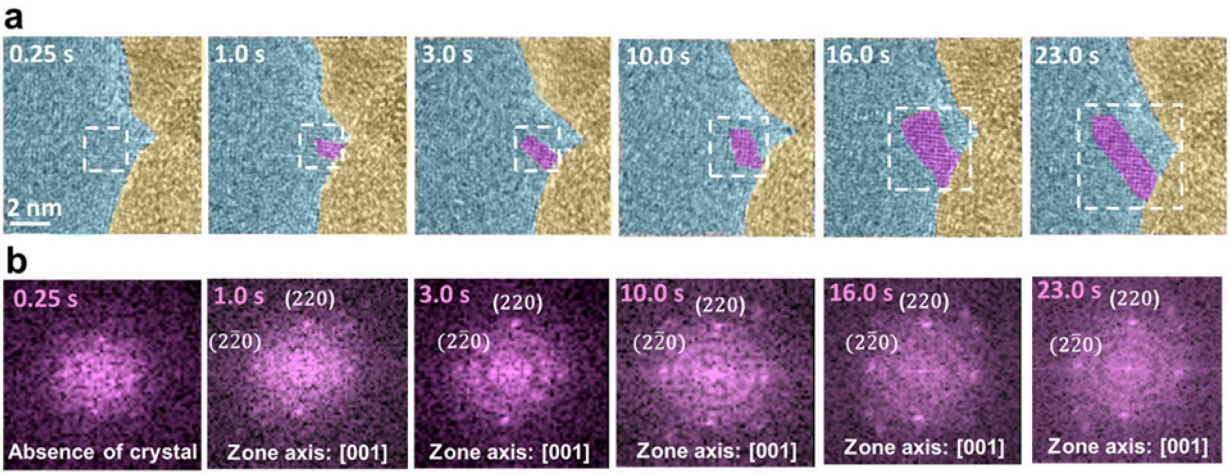

Figure 2. In-situ liquid TEM heterogeneous ice nucleation at a TiO_2-water nanointerface within a GLC on a TEM holder at cryogenic temperatures. (a) Time-sequenced TEM micrographs indicate single ice crystal nucleation and growth events. (b) FFT analysis at each instance confirms the cubic phase of ice. TiO_2 nanoparticles, ice, and water have been false-colored in gold, purple, and cyan, respectively, for better visualization.

Video S4 shows ice crystal growth by oriented attachment of ice nuclei at low temperatures. Ice surface attachment kinetics are important in the understanding of the interfacial dynamics processes, which define how free water molecules attach to the ice surface lattice.[41] During ice crystal growth, the latent heat of fusion affects the crystal surface temperature, while its diffusion limits the crystal growth.[42] Cubic ice phase is a well-known metastable phase, which can easily transition to a hexagonal stable phase by increasing temperature above -123°C.[43] According to a TEM SAED study, the cubic phase of ice can be found within the temperature range -130°C to -160°C, whereas the stable hexagonal ice phase is formed between -90°C and -100°C.[17] Shilling *et al.* showed that metastable cubic phase of ice exists at a 10% higher vapor pressure than hexagonal ice phase.[44] **Figure 3** shows time-sequenced micrographs of oriented attachment and growth of ice crystals nuclei close to the TiO_2-water interface. Recently, Zhang *et al.*[45] showed oriented growth of single ice crystal lamellar platelets in polymeric aqueous solutions, where freezing parameters controlling the velocity of crystal growth were discussed. The present work emphasizes the behaviour of multiple nanoscale ice nuclei and ice crystal growth by an oriented attachment mechanism. **Figure 3a** shows false-colored TEM micrographs of the progression of ice crystal growth by oriented attachment. **Figure 3b** and **Figure 3c** show the corresponding FFT analyses from regions **R1** and **R2**, respectively. Region **R2** highlights the homogeneously grown ice crystal nucleus. FFT analysis confirms that all ice crystals underwent a metastable cubic phase. Both the heterogeneously and homogeneously grown ice crystals were observed to have a dominant crystal growth by oriented attachment. In region R1 at the TiO_2-water nanointerface, ice crystals undergo attachment and growth events by maintaining the crystal zone axis along the [001] direction. In region **R1**, from 9s to 49s two adjoining

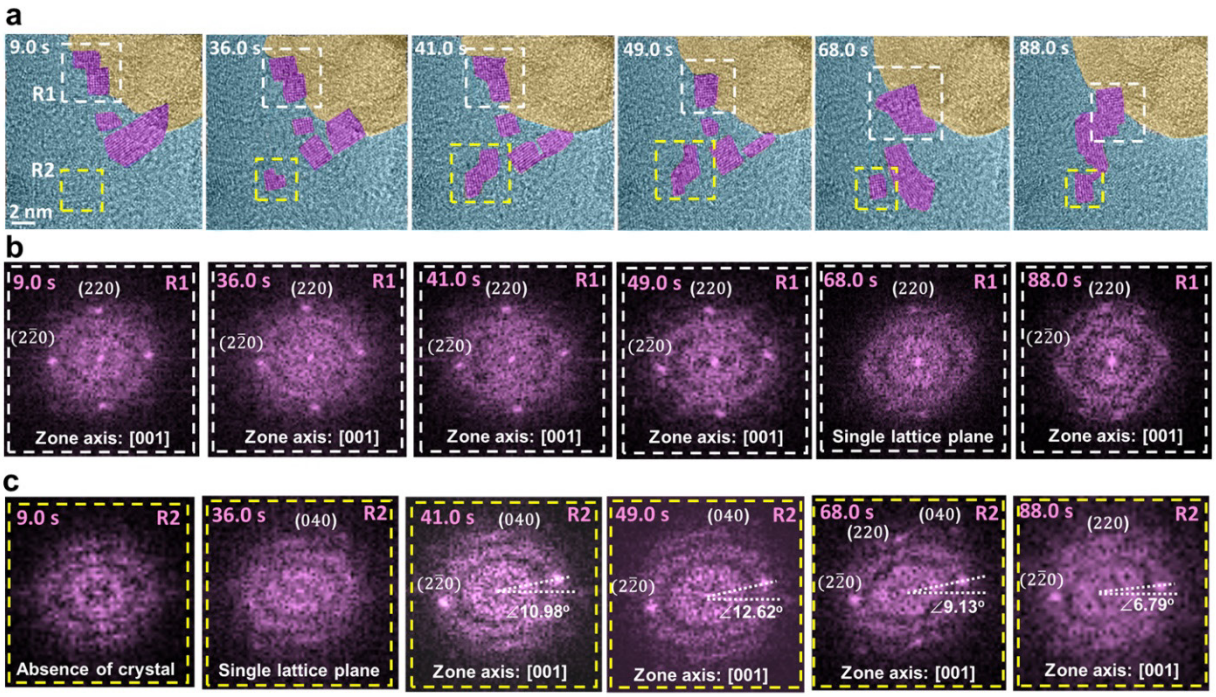

Figure 3. Ice crystal growth via oriented attachment in proximity to the TiO_2-water interface in GLC at cryogenic temperatures. (a) Time-sequenced TEM micrographs indicating multiple ice nuclei growing via oriented attachment. TiO_2 nanoparticles, ice, and water have been false-colored in gold, purple, and cyan, respectively, for better visualization. Region 1 (R1) shows ice crystal growth from oriented attachment of the existing nuclei. Region 2 (R2) indicates the progression from ice crystal nucleation to growth. (b) FFT analysis of ice crystals from R1, confirming the stability of cubic phase of ice nuclei over the period. (c) FFT analysis of ice crystals from R2, confirming the stability of cubic phase of ice nuclei over the period after oriented attachment.

ice crystals merge along the (220) facets. In region **R2**, no ice crystal nucleus was observed in the imaging focal plane at 9s. From 36s to 49s, preferential growth of ice crystals was observed. At 88s, both the homogeneously and heterogeneously nucleated ice crystals underwent coalescence to form a larger ice crystal. While slight reorientation of the ice nuclei appeared in region **R2** at 88s, eventually the nuclei reach a stable oriented attachment at the TiO_2-water nanointerface. This observation of ice crystal growth by oriented attachment at the TiO_2-water nanointerface suggests the presence of Van der Waals or hydrogen bonding interactions between ice crystals.[46] Nevertheless, the key events of such interactions need further investigation to be fully elucidated.

The effectiveness of radical scavenging properties of TiO_2 is demonstrated in **Figure 4**. **Video S5** shows the electron beam-induced dissolution events of ice crystals at distances away from the TiO_2 nanoparticle surface. The time-sequenced TEM micrographs in **Figure 4** represent the electron beam-induced degeneration events of ice crystals after 45 minutes of beam exposure. During *in-situ* GLC-TEM, after prolonged exposure to an electron beam, radiolysis by-products such as hydrated electrons (e^-), hydrated protons (H^+), hydroxyl radicals ($OH^\cdot$)**,** and hydrogen peroxide (H_2O_2) can be produced.[23] Xu *et al.*[47] showed that the two major mechanisms, namely, electron beam-induced local heating and movement of water molecules can cause melting of ice crystals. McMullan *et al.*[48] reported that for every incident electron ($e^-/Å^2$) water molecules can be displaced by 1 Å. In **Figure 4a**, TEM time-sequenced

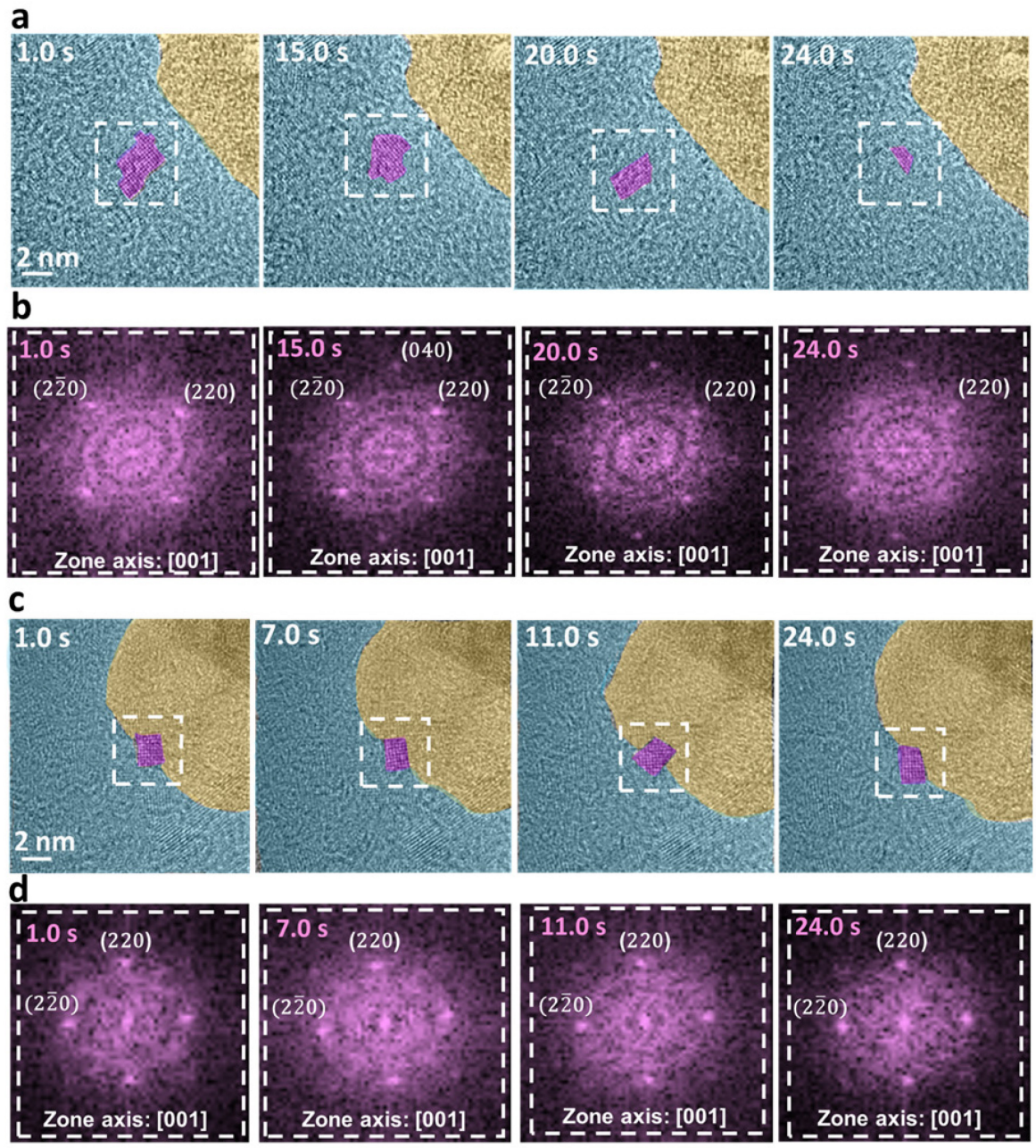

Figure 4. Ice crystal dissolution events at the TiO_2-water nanointerface and away from the nanointerface in GLC, observed after 45 minutes of electron beam exposure at cryogenic temperatures. (a) Time-sequenced TEM micrographs of ice crystal dissolution away from the TiO_2 nanoparticle interface, confirming the gradual reduction in crystal size. (b) Corresponding FFT analysis from highlighted region shows the diffused cubic phase ice crystal planes. (c) Time-sequenced TEM micrographs of an ice crystal formed at the TiO_2 nanoparticle surface, confirming the ice crystal's stability. (d) Corresponding FFT analysis from white-boxed region shows the stable cubic ice phase crystal. TiO_2 nanoparticles, ice, and water have been false-colored in gold, purple, and cyan, respectively, for better visualization in (a) and (c).

micrographs of an ice crystal dissolution in a GLC aqueous environment is represented. One can observe that the ice crystal size was significantly reduced after 24 s. The corresponding FFT reciprocal space analysis is shown in **Figure 4b**, where reduced intensity of FFT spots indicating lattice planes can be observed. **Figure 4c** represents the electron beam effect on an ice crystal formed at

the TiO_2-water nanointerface. Within the same time frame of 24 s, the ice crystal remained considerably stable without undergoing dynamic dissolution. The confirmation of a stable cubic crystal phase can be observed in the corresponding FFT fields in **Figure 4d**, where the (220) family of lattice planes along the [001] zone axis was consistent. **Video S6** shows the stable crystal at the TiO_2-water nanointerface after prolonged exposure to the electron beam. The enhanced stability of the ice crystals at the TiO_2-water nanointerface points to the scavenging effect of TiO_2 nanoparticles.[29] **Video S7** shows there were no ice crystals observed at gold (Au) nanoparticle-water nanointerface under the same cryogenic temperature conditions in the GLC. **Figure S5** in the supporting information shows time-sequenced TEM micrographs of Au nanoparticles in the GLC aqueous environment, and reveals the absence of ice crystals. The present results indicate that the efficient scavenging ability and hydrophilic nature of TiO_2 nanoparticles under the electron beam in comparison to the Au nanoparticles, with the former possibly promoting stable nucleation and growth of ice crystals.

Dynamic processes associated with ice crystals melting govern a wide range of phenomena in nature and in our day-to-day life. Three primary mechanisms of ice melting associated with the global warming include reduced water heat capacity by solutes, strain heating, and granular basal sliding.[49] The surface properties of ice and the first order phase transitions are determined by the quasi-liquid layers (QLLs) that appear at temperatures below the ice melting point.[50, 51] The QLLs play an important role in cryo-preservation, regelation, slipperiness, recrystallization and coarsening of ice grains, glaciology, and atmospheric science.[51] A variety of experimental techniques have been utilized to investigate the ice surface melting layers, including atomic force microscopy, photoelectron spectroscopy, ellipsometry, etc.[52-54] The present study illustrates the electron beam-induced nanoscale melting dynamics of ice crystal nuclei. These direct observations that confirm the stability of ice crystal nuclei at the radical scavenger TiO_2 and water nanointerface may also be used to devise novel strategies to control ice melting.

Conclusions

The present work demonstrated the potential of radical scavengers for *in-situ* GLC-TEM studies of ice crystal formation and growth. Specifically, the work explored real-time nucleation of ice crystals in the presence of radical-scavenging TiO_2 nanoparticles immersed in water at cryogenic temperatures. Interestingly, both heterogeneously and homogeneously grown ice crystals showcased cubic crystal structure. The cubic ice crystal phase was consistently observed during nucleation and growth events, where {220} family of lattice planes corresponding to 2.2 Å d-spacings were present. The heterogeneous ice nucleation at the TiO_2-water nanointerface was observed to grow along the $[2\bar{2}0]$ direction while maintaining the [001] zone axis. The present results show that ice crystals predominantly grow via an oriented attachment mechanism, suggesting the presence of Van der Waals or hydrogen bonding interactions between ice crystals. Under prolonged exposure to electron beam, homogeneously formed ice crystals eventually dissolve, although ice crystals at the TiO_2-water nanointerface remained stable.

Author Contributions

R.S.Y., T.S. and C.M.M. conceptualized and supervised the study. A.H.P. performed in-situ GLC TEM experiments and analysed the results. A.H.P. and R.S.Y. wrote the manuscript. All authors proofread, commented on, and approved the final manuscript for submission.

Conflicts of interest

There are no conflicts to declare.

Acknowledgements

The present work made use of instruments in the Electron Microscopy Core of the Research Resources Centre at The University of Illinois Chicago. This material is based upon work supported by the National Science Foundation under Grants DMR-1809439 to R. Shahbazian-Yassar, CBET-1805753 to C. Megaridis and DMR-1710049 to T. Shokuhfar.

References

1. S. G. Cober, G. A. Isaac and J. W. Strapp, *Journal of Applied Meteorology*, 2001, **40**, 1984-2002.
2. P. J. DeMott, D. C. Rogers and S. M. Kreidenweis, *Journal of Geophysical Research: Atmospheres*, 1997, **102**, 19575-19584.
3. C. A. Knight, A. L. De Vries and L. D. Oolman, *Nature*, 1984, **308**, 295-296.
4. C. E. Morris, D. G. Georgakopoulos and D. C. Sands, *Journal de Physique IV (Proceedings)*, 2004, **121**, 87-103.
5. M. A. Freedman, *The Journal of Physical Chemistry Letters*, 2015, **6**, 3850-3858.
6. N. Eltouny and P. A. Ariya, *AIP Conference Proceedings*, 2013, **1527**, 930-932.
7. B. Murray, D. O'sullivan, J. Atkinson and M. Webb, *Chemical Society Reviews*, 2012, **41**, 6519-6554.
8. R. Souda, T. Aizawa, N. Sugiyama and M. Takeguchi, *Physical Chemistry Chemical Physics*, 2020, **22**, 20515-20523.
9. M. A. Henderson, *Surface Science Reports*, 2002, **46**, 1-308.
10. K. Onda, B. Li, J. Zhao, K. D. Jordan, J. Yang and H. Petek, *Science*, 2005, **308**, 1154-1158.
11. A. Kiselev, F. Bachmann, P. Pedevilla, S. J. Cox, A. Michaelides, D. Gerthsen and T. Leisner, *Science*, 2017, **355**, 367-371.
12. L. Jia, W. Cui, Y. Chen, Y. Li and J. Li, *International Journal of Heat and Mass Transfer*, 2018, **120**, 909-913.
13. S. J. Cox, S. M. Kathmann, B. Slater and A. Michaelides, *The Journal of chemical physics*, 2015, **142**, 184704.
14. L. Lupi, B. Peters and V. Molinero, *The Journal of chemical physics*, 2016, **145**, 211910.
15. G. C. Sosso, T. Li, D. Donadio, G. A. Tribello and A. Michaelides, *The journal of physical chemistry letters*, 2016, **7**, 2350-2355.
16. A. Falls, S. Wellinghoff, Y. Talmon and E. Thomas, *Journal of materials science*, 1983, **18**, 2752-2764.
17. M. Kumai, *Journal of Glaciology*, 1968, **7**, 95-108.
18. A. Kouchi, M. Tsuge, T. Hama, Y. Oba, S. Okuzumi, S.-i. Sirono, M. Momose, N. Nakatani, K. Furuya and T. Shimonishi, *The Astrophysical Journal*, 2021, **918**, 45.
19. R. Kato, Y. Hatano, N. Kasahata, C. Sato, K. Suenaga and M. Hasegawa, *Carbon*, 2020, **160**, 107-112.
20. S. M. Ghodsi, C. M. Megaridis, R. Shahbazian-Yassar and T. Shokuhfar, *Small Methods*, 2019, **3**, 1900026.
21. N. Mohanty, M. Fahrenholtz, A. Nagaraja, D. Boyle and V. Berry, *Nano letters*, 2011, **11**, 1270-1275.
22. E. Firlar, M. Ouy, A. Bogdanowicz, L. Covnot, B. Song, Y. Nadkarni, R. Shahbazian-Yassar and T. Shokuhfar, *Nanoscale*, 2019, **11**, 698-705.
23. C. Wang, T. Shokuhfar and R. F. Klie, *Advanced Materials*, 2016, **28**, 7716-7722.
24. G. Algara-Siller, O. Lehtinen, F. Wang, R. R. Nair, U. Kaiser, H. Wu, A. K. Geim and I. V. Grigorieva, *Nature*, 2015, **519**, 443-445.
25. F. Wang, H. Wu and A. Geim, *Nature*, 2015, **528**, E3-E3.
26. W. Zhou, K. Yin, C. Wang, Y. Zhang, T. Xu, A. Borisevich, L. Sun, J. C. Idrobo, M. F. Chisholm and S. T. Pantelides, *Nature*, 2015, **528**, E1-E2.
27. N. M. Schneider, M. M. Norton, B. J. Mendel, J. M. Grogan, F. M. Ross and H. H. Bau, *The Journal of Physical Chemistry C*, 2014, **118**, 22373-22382.
28. S. M. Ghodsi, S. Anand, R. Shahbazian-Yassar, T. Shokuhfar and C. M. Megaridis, *ACS nano*, 2019, **13**, 4677-4685.
29. H. Xie, X. Xie, G. Hu, V. Prabhakaran, S. Saha, L. Gonzalez-Lopez, A. H. Phakatkar, M. Hong, M. Wu and R. Shahbazian-Yassar, *Nature Energy*, 2022, **7**, 281-289.
30. J. J. Carey and K. P. McKenna, *The Journal of Physical Chemistry C*, 2019, **123**, 22358-22367.
31. M. Canillas, E. Chinarro, M. Freitas, A. P. Pêgo and B. Moreno, *Journal of Catalysis*, 2020, **381**, 186-192.
32. H. Cho, M. R. Jones, S. C. Nguyen, M. R. Hauwiller, A. Zettl and A. P. Alivisatos, *Nano letters*, 2017, **17**, 414-420.
33. Y. Qiu, Z. Wang, A. C. Owens, I. Kulaots, Y. Chen, A. B. Kane and R. H. Hurt, *Nanoscale*, 2014, **6**, 11744-11755.

34. Y. Morita, S. Suzuki, K. Sato and T. Takui, *Nature chemistry*, 2011, **3**, 197-204.
35. N. Cho and J. Hallett, *Journal of crystal growth*, 1984, **69**, 317-324.
36. T. Croteau, A. Bertram and G. Patey, *The Journal of Physical Chemistry A*, 2008, **112**, 10708-10712.
37. M. Fitzner, G. C. Sosso, S. J. Cox and A. Michaelides, *Journal of the American Chemical Society*, 2015, **137**, 13658-13669.
38. J. Hallett, *Journal of Atmospheric Research* 1972, **6**, 223-236.
39. C. Marcolli, *Atmospheric Chemistry and Physics*, 2014, **14**, 2071-2104.
40. L. Lupi, A. Hudait, B. Peters, M. Grünwald, R. Gotchy Mullen, A. H. Nguyen and V. Molinero, *Nature*, 2017, **551**, 218-222.
41. K. G. Libbrecht, *Annu. Rev. Mater. Res*, 2017, **47**, 271-295.
42. A. S. Michaels, P. Brian and P. R. Sperry, *Journal of Applied Physics*, 1966, **37**, 4649-4661.
43. T. Hansen, M. Koza, P. Lindner and W. Kuhs, *Journal of Physics: Condensed Matter*, 2008, **20**, 285105.
44. J. Shilling, M. Tolbert, O. Toon, E. Jensen, B. J. Murray and A. K. Bertram, *Geophysical research letters*, 2006, **33**.
45. T. Zhang, L. Wang, Z. Wang, J. Li and J. Wang, *The Journal of Physical Chemistry B*, 2021, **125**, 970-979.
46. X. Xue, R. L. Penn, E. R. Leite, F. Huang and Z. Lin, *CrystEngComm*, 2014, **16**, 1419-1429.
47. H. Xu, J. Ångström, T. Eklund and K. Amann-Winkel, *The Journal of Physical Chemistry B*, 2020, **124**, 9283-9288.
48. G. McMullan, K. Vinothkumar and R. Henderson, *Ultramicroscopy*, 2015, **158**, 26-32.
49. D. Ren and L. M. Leslie, *Journal of Glaciology*, 2011, **57**, 1057-1066.
50. Y. Li and G. A. Somorjai, *The Journal of Physical Chemistry C*, 2007, **111**, 9631-9637.
51. G. Sazaki, S. Zepeda, S. Nakatsubo, M. Yokomine and Y. Furukawa, *Proceedings of the National Academy of Sciences*, 2012, **109**, 1052-1055.
52. H. Bluhm, D. F. Ogletree, C. S. Fadley, Z. Hussain and M. Salmeron, *Journal of Physics: Condensed Matter*, 2002, **14**, L227.
53. A. Döppenschmidt and H.-J. Butt, *Langmuir*, 2000, **16**, 6709-6714.
54. Y. Furukawa, M. Yamamoto and T. Kuroda, *Journal of crystal growth*, 1987, **82**, 665-677.